Finite element approximation of coupled seismic and electromagnetic waves in gas hydrate-bearing sediments

Juan E. Santos[†]

[†] CONICET, Departamento de Geofísica Aplicada,

Facultad de Ciencias Astronómicas y Geofísicas, Universidad Nacional de La Plata

and Department of Mathematics, Purdue University.

Joint work with Fabio I. Zyserman and Patricia M. Gauzellino

2009 SIAM Annual Meeting , Denver, Colorado, July 6-10 2009

Electroseismic Modeling. I

Within a fluid saturated porous medium there exists a nanometer-scale separation of electric charge in which a bound charge existing on the surface of the solid matrix (normally of negative sign) is balanced by adsorbed positive ions of the surrounding fluid, setting an immobile double (Stern) layer, having a thickness of about 10 nm.

Electroseismic Modeling. II

Further from the surface of the solid matrix there exists a distribution of mobile counter ions, forming the so called **diffuse layer**. When an electric field is applied to this system, the ions in the diffuse layer move, dragging the pore fluid along with it because of the **viscous traction**. This is known as **electro-osmosis** and is responsible for the **electroseismic phenomena**.

Electroseismic Modeling. III

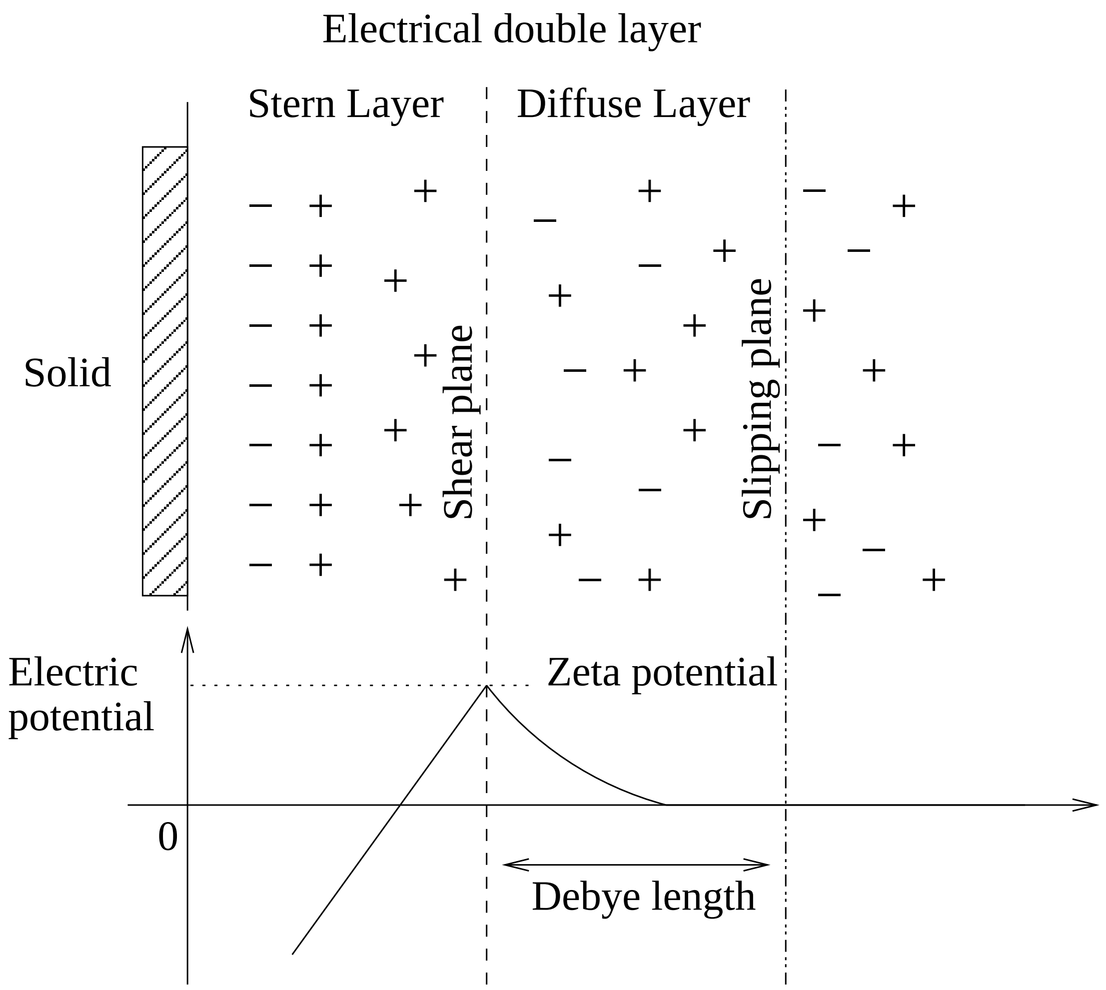

2D Model and Sources. I

Assume that the subsurface is an horizontally layered fluid-saturated porus medium.

Consider two different electromagnetic sources, both in the y-direction:

1) an infinite current line J_e^{ext},

2) an infinite magnetic dipole (infinite solenoid) J_m^{ext}.

2D Model and Sources. II

J_m^{ext} induces electromagnetic fields $(E_x(x,z), E_z(x,z))$, and $H_y(x,z)$, and fluid and solid displacements $(u_x^s(x,z), u_z^s(x,z))$ and $(u_x^f(x,z), u_z^f(x,z))$, respectively.

This is known as the PSVTM-mode, in which compressional and vertically polarized shear seismic waves (PSV-waves) are present.

2D Model and Sources. III

J_e^{ext} induces electromagnetic fields $(H_x(x,z), H_z(x,z))$ and $E_y(x,z)$, and fluid and solid displacements $u_y^s(x,z)$ and $u_y^f(x,z)$, respectively.

This is known as the SHTE-mode, where only horizontally polarized seismic waves (SH-waves) are present.

2D Model and Sources. IV

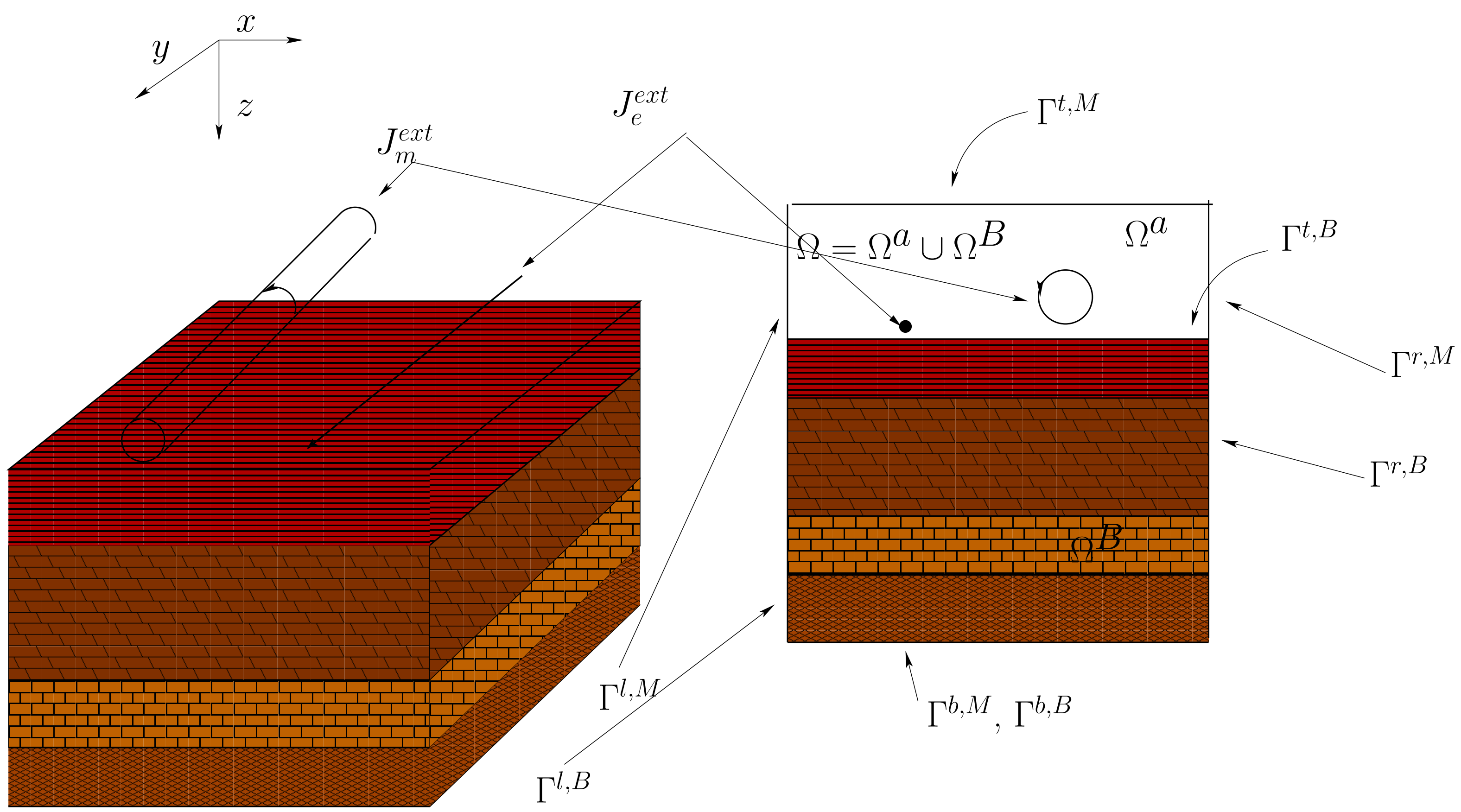

3D layered subsurface, 2D model $\Omega = \Omega^a \cup \Omega^B$ and electromagnetic sources.

Formulation in Terms of Scattered Fields E^s, H^s. PSVTM-mode.

Let

$$\sigma(x,z) = \sigma^p(z) + \sigma^s(x,z),$$

$\sigma^p(z)$: background conductivity, $\sigma^s(x,z)$: conductivity anomaly.

Let $E^s = E - E^p$, $H^s = H - H^p$: scattered fields.

For the PSVTM-mode, solve for the primary fields E^p, H^p solution of:

$$\nabla \times E^p = -i\omega\mu H^p + J_m^s, \quad \text{in} \quad \Omega,$$
$$\nabla \times H^p = \sigma^p E^p, \quad \text{in} \quad \Omega.$$

Analytical expressions for E^p, H^p are known for the case that Ω is the whole space R^3 and σ_p is constant.

Differential Model for the PSVTM-mode. I

In terms of the scattered electromagnetic fields the equations for PSVTM electroseismic modeling are (Pride, 1994):

$$\sigma E^s - \mathrm{curl} H_y^s = -\sigma^s E^p, \quad \Omega,$$

$$\mathrm{curl} E^s + i\omega\mu H_y^s = 0, \quad \Omega,$$

$$-\omega^2 \rho_b u^s - \omega^2 \rho_f u^f - \nabla \cdot \tau(u) = 0, \quad \Omega^B,$$

$$-\omega^2 \rho_f u^s + \eta(\kappa(\omega))^{-1} i\omega u^f + \nabla p_f$$

$$= \eta(\kappa(\omega))^{-1} L(\omega) \left(E^p + E^s\right), \ \ \Omega^B,$$

$$\tau_{lm}(u) = 2N\, \varepsilon_{lm}(u^s) + \delta_{lm} \left(\lambda_c \nabla \cdot u^s - \alpha K_{av}\, \xi\right),$$

$$p_f(u) = -\alpha K_{av} \nabla \cdot u^s + K_{av} \xi.$$

$\tau_{lm}(u)$: stress tensor, $p_f(u)$: fluid pressure.

Differential Model for the PSVTM-mode. II

$L(\omega)$: complex coupling coefficient, depending on the effective permeability, porosity, fluid permittivity and salinity among other parameters.

$\kappa(\omega)$: Dynamic permeability:

$$\kappa(\omega) = \kappa_0 \left[\left(1 + i \frac{\omega}{\omega_c} \frac{4}{m} \right)^{\frac{1}{2}} + i \frac{\omega}{\omega_c} \right]^{-1} = \kappa_r(\omega) - i \kappa_i(\omega),$$

κ_0: effective permeability

m: dimensionless parameter in the range $4 \leq m \leq 8$.

The electroseismic equations were solved employing absorbing boundary conditions at the artificial boundaries.

Weak Formulation for the PSVTM-mode. I

Find $(E^s, H^s_y, u^s, u^f) \in H(\text{curl}, \Omega) \times L^2(\Omega) \times [H^1(\Omega_B)]^2 \times H(\text{div}, \Omega_B)$ such that

$$
\begin{aligned}
&(\sigma E^s, \psi) - (H^s_y, \text{curl}\psi) + \langle a(1-i)E^s \cdot \chi, \psi \cdot \chi \rangle + (\text{curl}E^s, \varphi) + (i\omega\mu H^s_y, \varphi) \\
&\quad = -\left(\sigma^s E^p, \psi\right), \quad (\psi, \varphi) \in H(\text{curl}, \Omega) \times L^2(\Omega)
\end{aligned}
$$

$$
\begin{aligned}
&-\omega^2 \left(\rho_b u^s, v^s\right)_{\Omega_B} - \omega^2 \left(\rho_f u^f, v^s\right)_{\Omega_B} - \omega^2 \left(\rho_f u^s, v^f\right)_{\Omega_B} + \left(\eta(\kappa(\omega))^{-1} i\omega u^f, v^f\right)_{\Omega_B} \\
&+ \sum_{l,m} \left(\tau_{lm}(u), \varepsilon_{lm}(v^s)\right)_{\Omega_B} - \left(p_f(u), \nabla \cdot v^f\right)_{\Omega_B} + i\omega \left\langle \mathcal{D} S_{\Gamma_p}(u), S_{\Gamma_P}(v) \right\rangle_{\Gamma_p} \\
&\quad = \left(L(\omega)\eta(\kappa(\omega))^{-1}\left(E^p + E^s\right), v^f\right)_{\Omega_B}, \quad (v^s, v^f) \in [H^1(\Omega_B)]^2 \times H(\text{div}, \Omega_B). \\
&S_{\Gamma_p}(u) = \left(u^s \cdot \nu, u^s \cdot \chi, u^f \cdot \nu\right)
\end{aligned}
$$

ν: unit outer normal on $\Gamma_B = \partial\Omega_B$, χ: a unit tangent on Γ_B oriented counterclockwise,

$\mathcal{D}$: a positive definite matrix, $a = \left(\frac{\sigma}{2\omega\mu}\right)$

A Finite Element Procedure for the PSVTM-mode. I

$\mathcal{T}^h(\Omega)$: nonoverlapping partition of $\Omega = \Omega_a \cup \Omega_B$ into rectangles Ω_j of diameter bounded by h

For the electric vector E^s and the magnetic scalar H_y^s we use

$$\mathcal{V}^h = \{\psi \in H(\text{curl}, \Omega) : \psi|\Omega_j \in \mathcal{V}_j^h \equiv P_{0,1}(\Omega_j) \times P_{1,0}(\Omega_j)\},$$

$$\mathcal{W}^h = \{\varphi \in L^2(\Omega) : \varphi|\Omega_j \in \mathcal{W}_j^h \equiv P_0(\Omega_j)\}.$$

DOF: tangential componets of E^s at the mid points of the sides of each Ω_j and the value of H_y^s at the center of Ω_j.

A Finite Element Procedure for the PSVTM-mode. II

For each component of the solid displacement u^s we use the space $\mathcal{N}C^h$:

$$\widehat{R} = [-1,1]^2, \qquad \widehat{\mathcal{N}C}(\widehat{R}) = \text{Span}\{1, \hat{x}, \hat{z}, \widetilde{\alpha}(\hat{x}) - \widetilde{\alpha}(\hat{z})\}$$

$$\widetilde{\alpha}(\hat{x}) = \hat{x}^2 - \frac{5}{3}\hat{x}^4.$$

DOF: values of u^s at the midpoint of each edge of $\widehat{R}$.

$$\mathcal{N}C^h = \{v \,:\, v_j = v|_{\Omega_j} \in \mathcal{N}C^h(\Omega_j),\; v_j(\xi_{jk}) = v_k(\xi_{jk}) \;\forall (j,k)\}.$$

The space $\mathcal{N}C^h$ yields about half the numerical dispersion than that of standard bilinear elements.

A Finite Element Procedure for the PSVTM-mode. III

For the fluid displacement u^f vector we use:

$$\mathcal{M}^h = \{v \in H(\text{div}, \Omega_B) \, : v_j = v|_{\Omega_j} \in P_{1,0} \times P_{0,1}(\Omega_j)\}$$

DOF: value of $u^f \cdot \nu$ at the mid points of each side of Ω_j.

A Finite Element Procedure for the PSVTM-mode. IV

Find $(E^{s,h}, H_y^{s,h}, u^{s,h}, u^{f,h}) \in \mathcal{V}^h \times \mathcal{W}^h \times [\mathcal{N}C^h]^2 \times \mathcal{M}^h$ such that

$$(\sigma E^{s,h}, \psi) - (H_y^{s,h}, \text{curl}\psi) + \left\langle a(1-i)E^{s,h} \cdot \chi, \psi \cdot \chi \right\rangle$$
$$+(\text{curl} E^{s,h}, \varphi) + (i\omega\mu H_y^{s,h}, \varphi)$$
$$= -\left(\sigma^s E^p, \psi\right), \quad (\psi, \varphi) \in \mathcal{V}^h \times \mathcal{W}^h$$

$$-\omega^2 \left(\rho_b u^{s,h}, v^s\right)_{\Omega_B} - \omega^2 \left(\rho_f u^{f,h}, v^s\right)_{\Omega_B} - \omega^2 \left(\rho_f u^{s,h}, v^f\right)_{\Omega_B}$$
$$+ \left(\eta(\kappa(\omega))^{-1} i\omega u^{f,h}, v^f\right)_{\Omega_B} + \sum_{l,m} \left(\tau_{lm}(u^h), \varepsilon_{lm}(v^s)\right)_{\Omega_B}$$
$$- \left(p_f(u^h), \nabla \cdot v^f\right)_{\Omega_B} + i\omega \left\langle \mathcal{D} S_{\Gamma_p}(u^h), S_{\Gamma_P}(v)\right\rangle_{\Gamma_p}$$
$$= \left(L(\omega)\eta(\kappa(\omega))^{-1} \left(E^p + E^{s,h}\right), v^f\right)_{\Omega_B}, (v^s, v^f) \in [\mathcal{N}C^h]^2 \times \mathcal{M}^h.$$

A Priori Error Estimates for the PSVTM-mode.

A priori error estimate:

Theorem:

for $\omega > 0$ and sufficiently small $h > 0$,

$$
\begin{aligned}
&\|E^s - E^{s,h}\|_0 + \|\textbf{curl}(E^s - E^{s,h})\|_0 + \|H_y^s - H_y^{s,h}\|_0 \\
&\quad + \|u^s - u^{s,h}\|_{1,h,\Omega_B} + \|u^f - u^{f,h}\|_{0,\Omega_B} \\
&\quad + \|(E^s - E^{s,h}) \cdot \chi\|_{0,\Gamma} + \|u^s - u^{s,h}\|_{0,\Gamma_B} \\
&\qquad \leq C(\omega) \left[h \left(\|E^s\|_1 + \|\textbf{curl}\ E^s\|_1 + \|H_y^s\|_1 \right) \right. \\
&\qquad\qquad \left. + h^{1/2} \left(\|u^s\|_{2,\Omega_B} + \|u^f\|_{1,\Omega_B} + \|\nabla \cdot u^f\|_{1,\Omega_b} \right) \right].
\end{aligned}
$$

Numerical Electroseismic Modeling for the PSVTM-mode. I

Gas hydrates (GH) are crystalline molecular complexes composed of water and **natural gas, mainly methane**, which form under certain conditions of low temperature, high pressure and gas concentration. They are found in permafrost regions and seafloor sediments along the continental margins.

GH are ice-like structures within the pore space that cause strong changes in the **conductivity and phase velocities** of the seismic waves, making possible to detect its presence using electroseismic data.

Numerical Electroseismic Modeling for the PSVTM-mode. II

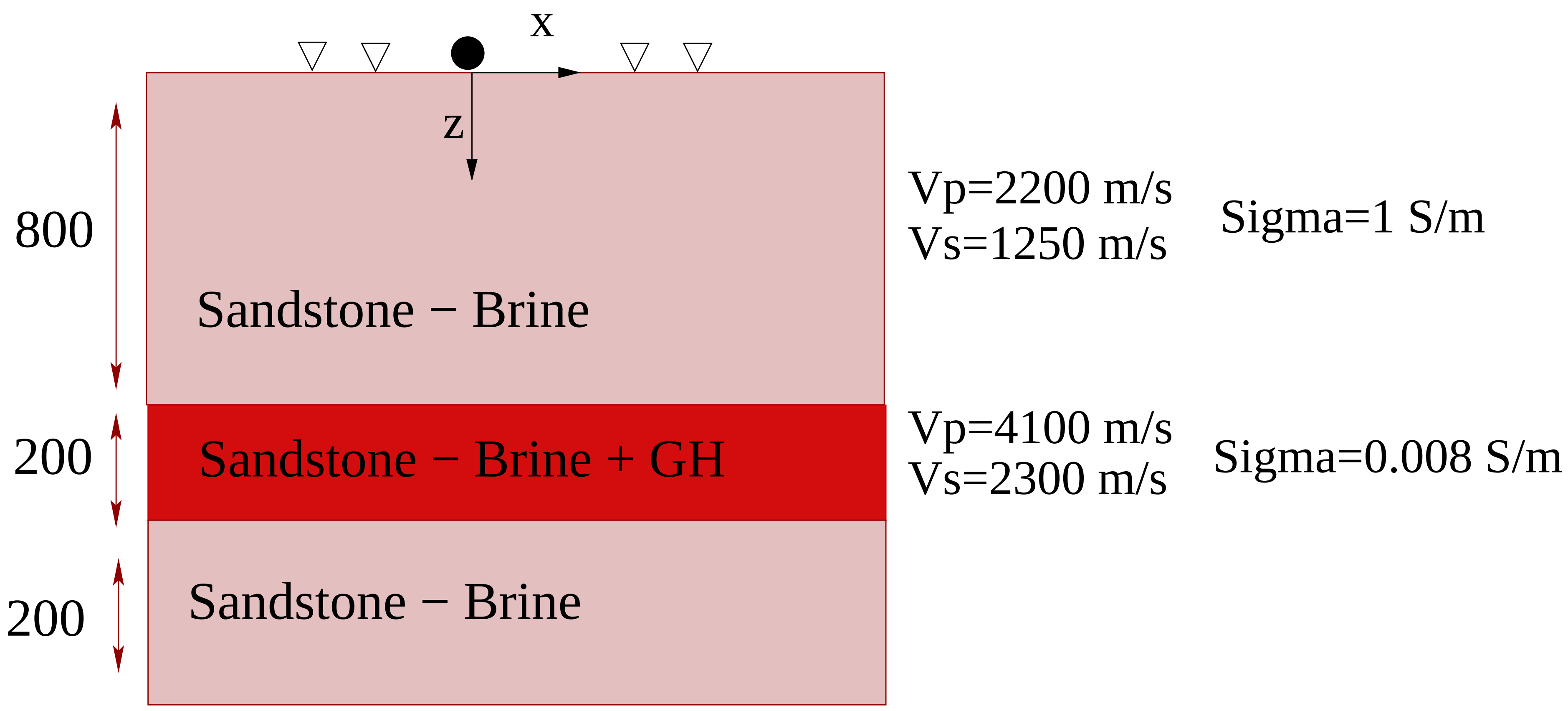

Brine-saturated sandstone subsurface model including a layer containing BRINE + GH in the pore space. The black dot at the top indicates the infinite solenoid source in the $y-$ direction located at $(x = 0, z = 0)$. The geophones are located near the earth surface, indicated with inverted triangles. Distances are given in meters. The model was discretized with a 2241×1121 mesh and solved for 100 frequencies with a main source frequency of 20 Hz. The reference mesh size was $h^* = 1.75$ m and the diffusion length at 20 Hz was 10 m. The CPU time running with 20 processors in the steele parallel computer at Purdue University was 7 hours.

z-component of solid acceleration (left) and fluid pressure (right) at t=0.2 s. GH-saturation $S_{gh} = 0.8$

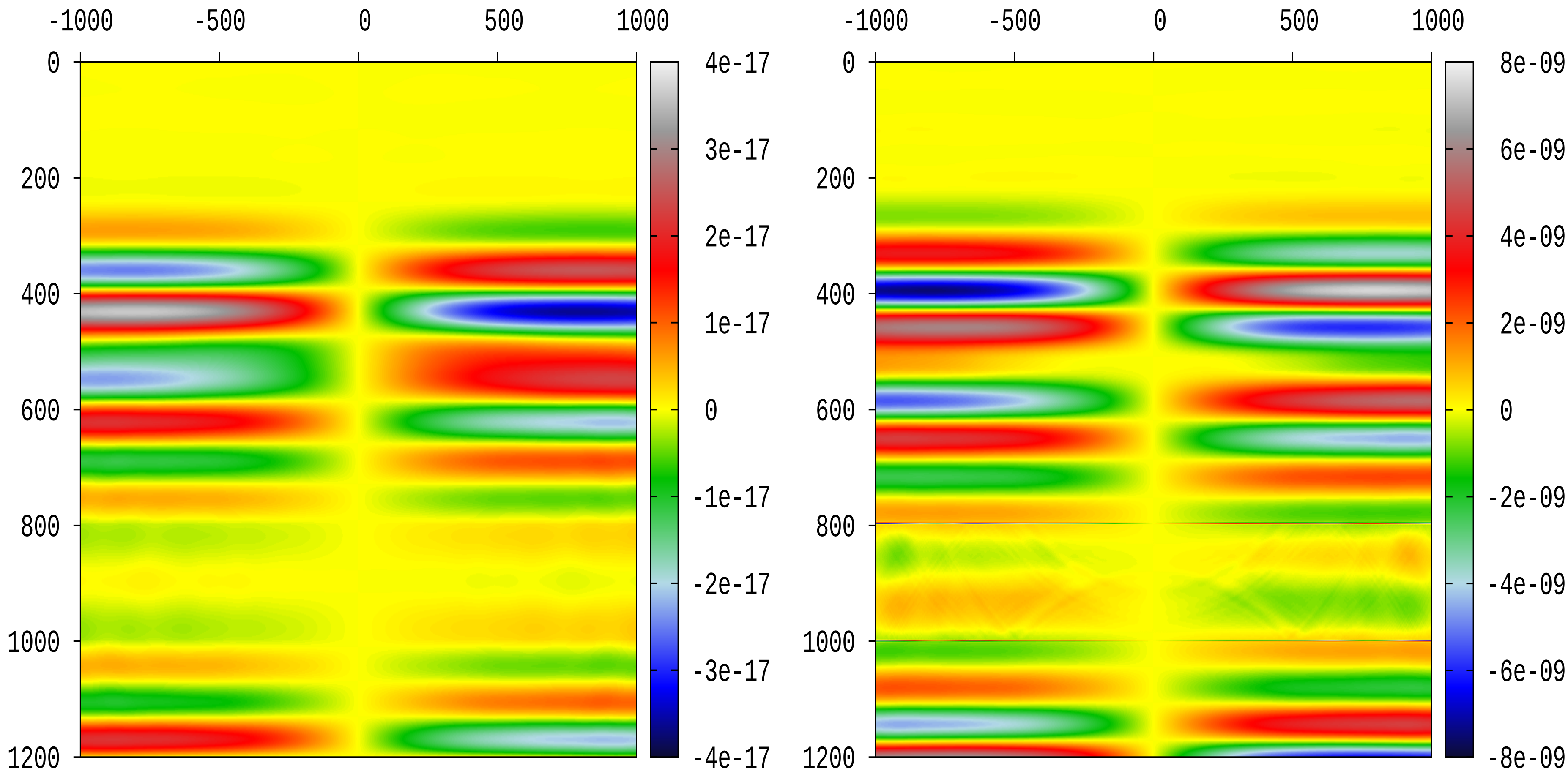

The snapshots show upward and downward travelling wavefronts generated by the presence of the the GH-bearing layer.

z-component of solid acceleration(left) and fluid pressure (right) at t=0.3 s. GH-saturation $S_{gh} = 0.8$

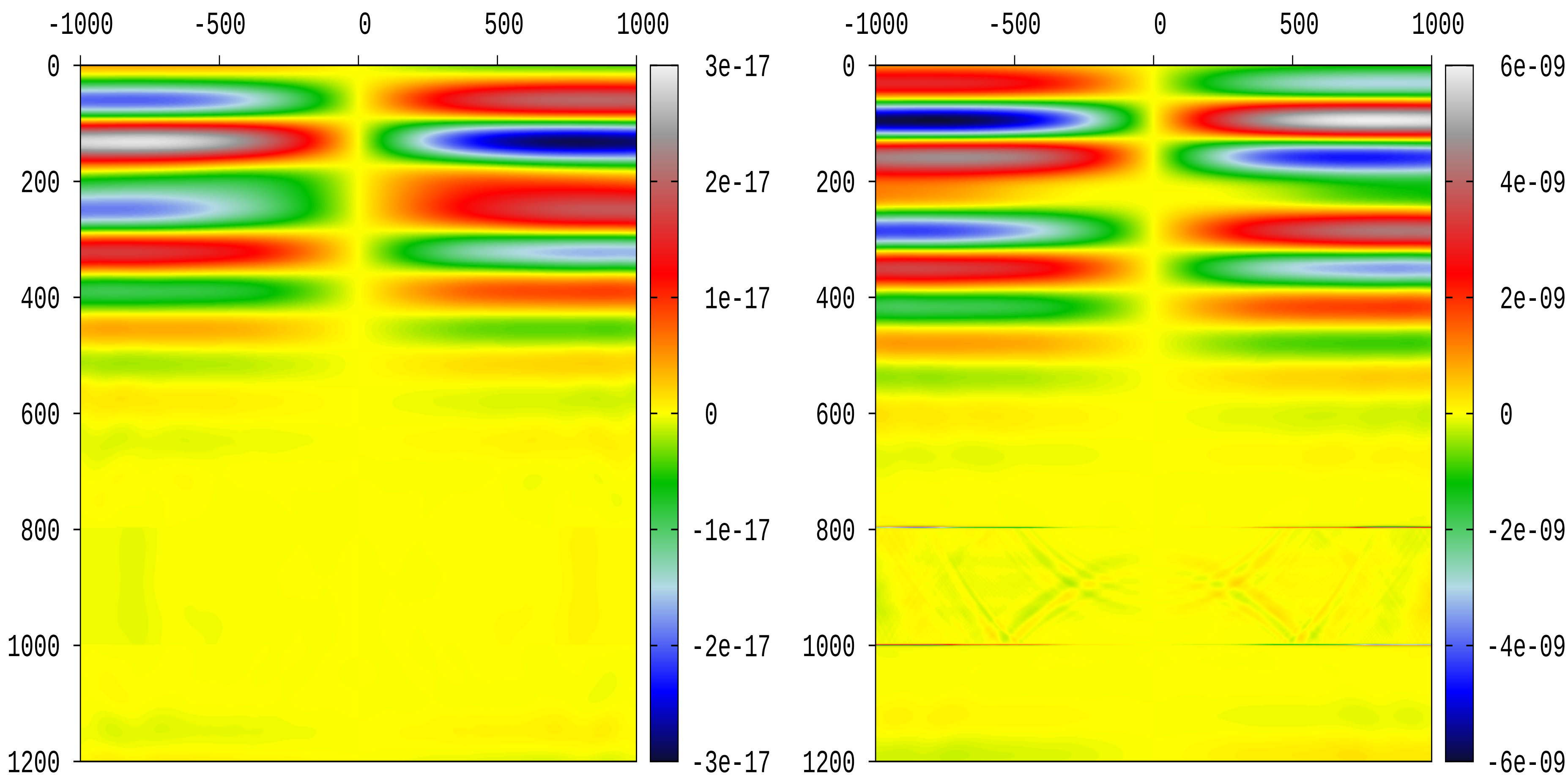

The snapshots show upward travelling wavefronts generated by the presence of the the GH-bearing layer.

Traces of z-component of solid acceleration for GH-saturation S_{gh}=0.8

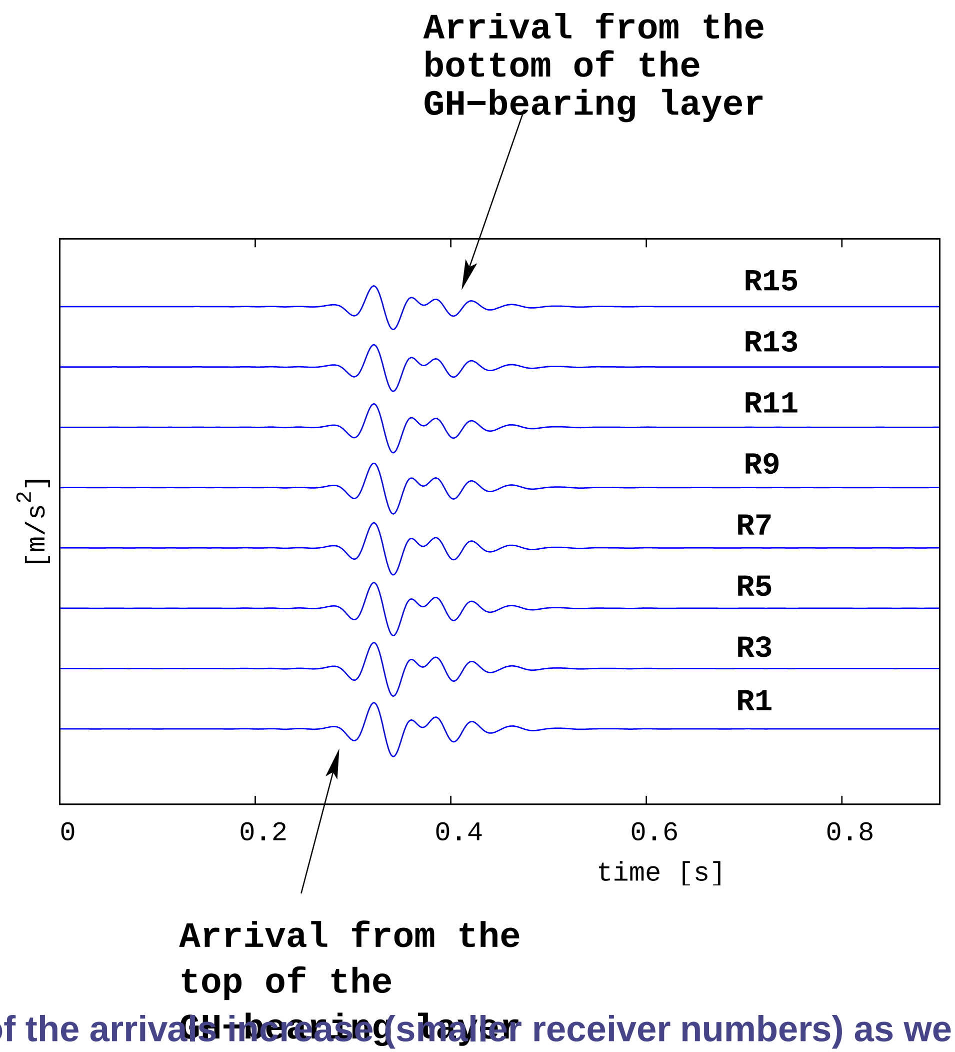

Notice that the amplitude of the arrivals increase (smaller receiver numbers) as we move away from the location of the infinite solenoide source located at x=0.

Traces of z-component of solid acceleration for different GH saturations

The electroseismic experiment is able to discriminate between different GH saturations

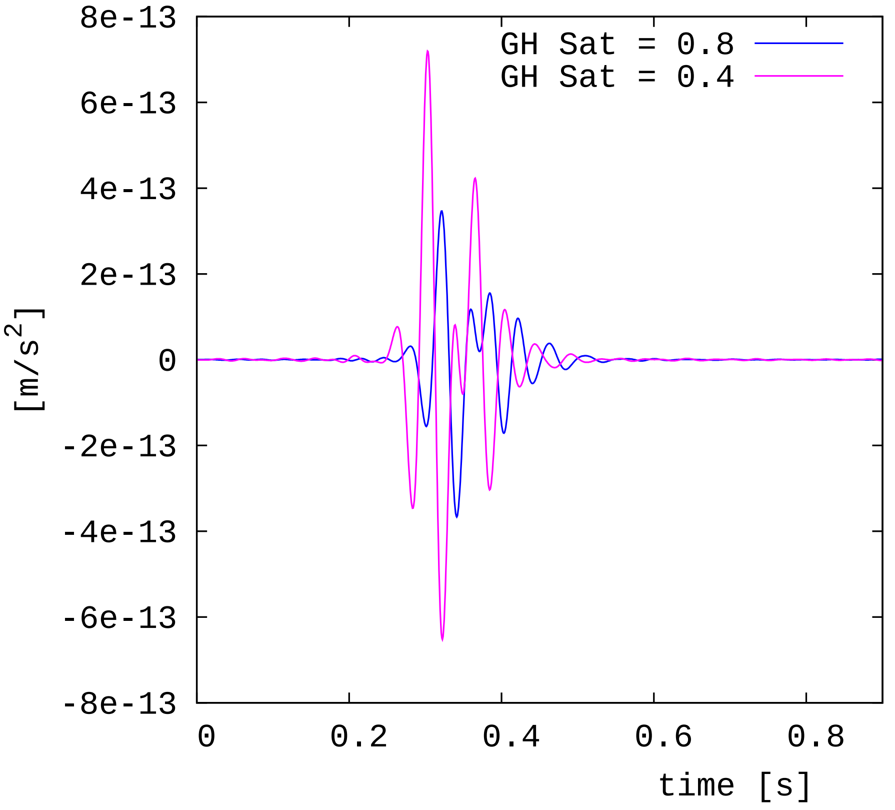

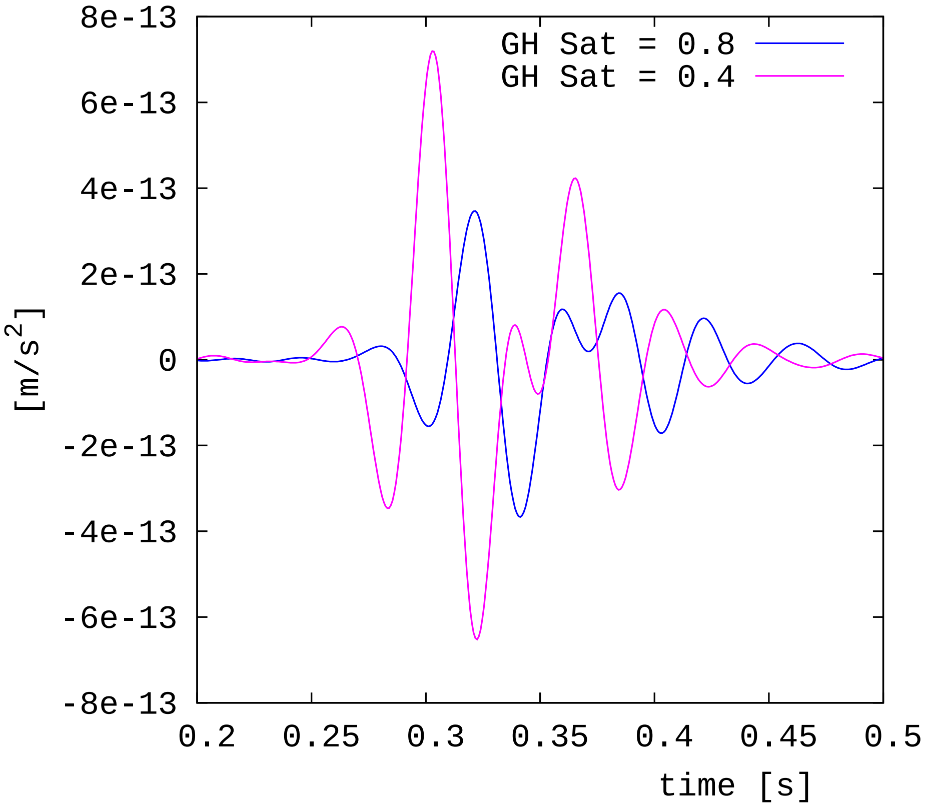

Traces of z-component of solid acceleration for different layer widths.

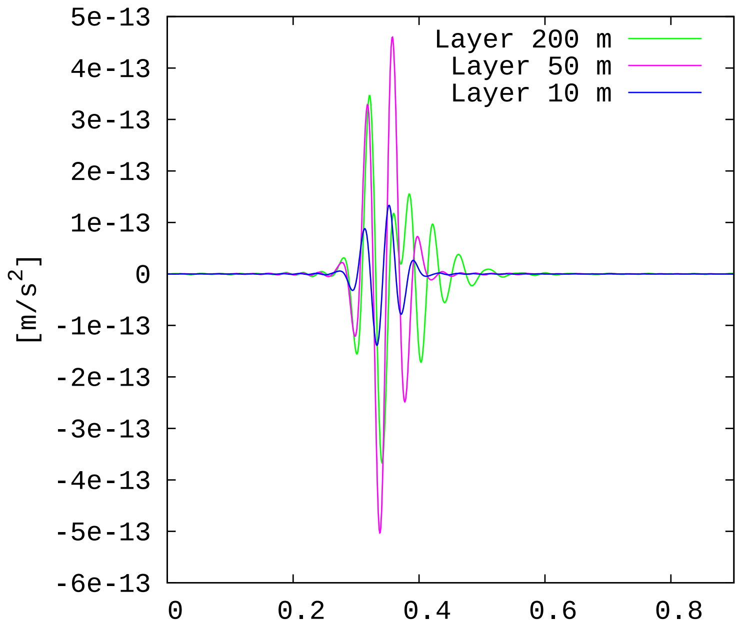

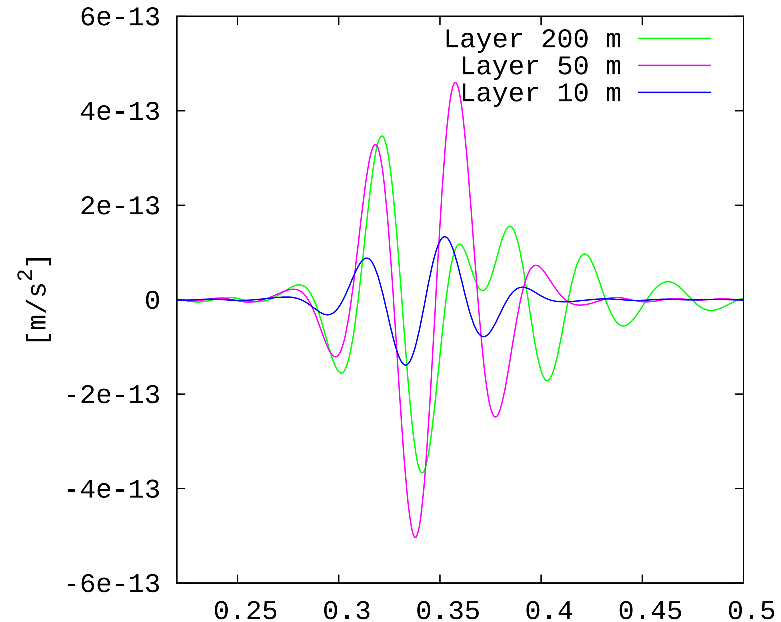

The arrival at t $\approx .3$ sec. is associated with wavefronts generated at the top of the GH-saturated layer. The 10 and 50 m width layers are seen as single reflectors. The second arrival at about .38 for the 200 m layer width case corresponds to the wavefront generated at the bottom of the GH bearing layer. Notice that a seismic source of the same frequency can not see the 10 m width layer.